High temperature ferromagnetism in single crystalline dilute Fe-doped $BaTiO_3$

Sugata Ray,[1,2,3,*] Priya Mahadevan,[4] Suman Mandal,[5] S. R. Krishnakumar,[5] Carlos Seiti Kuroda,[6] T. Sasaki,[7] Tomoyasu Taniyama,[1] and Mitsuru Itoh[1,†]

[1]*Materials and Structures Laboratory, Tokyo Institute of Technology, 4259 Nagatsuta, Midori-ku, Yokohama 226-8503, Japan*

[2]*Department of Materials Science, Indian Association for the Cultivation of Science, Jadavpur, Kolkata 700032, India*

[3]*Centre for Advanced Materials, Indian Association for the Cultivation of Science, Jadavpur, Kolkata 700032, India*

[4]*S. N. Bose National Center for Basic Sciences, JD Block, Sector III, Kolkata 700098, India*

[5]*Surface Physics Division, Saha Institute of Nuclear Physics, 1/AF Bidhannagar, Calcutta 700064, India*

[6]*Department of Innovative and Engineered Materials, Tokyo Institute of Technology, 4259 Nagatsuta, Midori-ku, Yokohama 226-8502, Japan*

[7]*National Institute for Materials Science, 1-2-1 Sengen, Tsukuba 305-0047, Japan*

(Received 7 November 2007; published 11 March 2008)

We report the observation of room temperature ferromagnetism in high quality, single crystalline dilute Fe-doped $BaTiO_3$. The large equilibrium solubility of Fe ions in the matrix refutes uncertainties about secondary phase magnetism, which has often eclipsed this interesting field of research. While room temperature ferromagnetism is observed at and above 5% Fe concentrations, one finds a highly concave temperature dependence of the susceptibility. Using detailed *ab initio* calculation, this has been related to intrinsic magnetic inhomogeneities arising from positional disorder. Apart from providing a mechanism for the observed high temperature ferromagnetism, our results point out that intrinsic disorder is a generic and essential component of dilute magnetism.

DOI: 10.1103/PhysRevB.77.104416 PACS number(s): 75.50.Pp, 61.72.J−, 71.20.−b, 77.22.−d

I. INTRODUCTION

Reports of high-T_c (Curie temperature) ferromagnetism in diluted magnetic oxide systems (DMOs) such as Co-doped TiO_2,[1] doped ZnO,[2] SnO_2,[3] and also undoped HfO_2 (Ref. 4) films within last few years have created lot of excitement, envisaging their future applications in the area of spintronics.[5] However, from the very beginning, these reports faced strong criticism because of the fact that transition metal solubilities in almost all the largely studied oxide matrices are invariably low, which not only restricted the experimental research in this field within the specially crafted thin film regime but also nurtured debates about possible dopant ion segregation, formation of ferromagnetic precipitates under certain growth conditions, etc.[6] Such uncertainties also acted as a setback for understanding the underlying mechanism for this unusual ferromagnetism and continued to demoralize the researchers. Evidently, it is essential to separate out the material related issues from the actual physics of this regime and in order to realize that, it is needed to search for systems with high dopant ion solubility that might even allow the growth of DMO samples in bulk single crystalline form. It is worth noting here that reports about single crystal DMOs are very rare, if not nonexistent altogether. Considering all these facts, we concentrated on insulating perovskite oxides and, consequently, succeeded to grow high quality single crystals of a DMO system exhibiting high temperature ferromagnetism. We are also able to provide a mechanism for the observed ferromagnetic properties, different from conventional ferromagnetism, with specific stress on few generic features of dilute magnetism. Our results also point out that the occurrence of dilute magnetism need not be restricted only to insulating binary oxide group of materials.

We have chosen Fe-doped $BaTiO_3$ as a possible candidate because $BaTiO_3$, a well-known ferroelectric oxide, is known to sustain a large concentration of transition metal dopant ion at the B site,[7–9] and single crystals could be easily grown using the floating zone method. Furthermore, there could be an interesting possibility of achieving mutiferroicity by a new and unusual route if dilute doped ferroelectric $BaTiO_3$ also develops ferromagnetism. We observe that the synthesized crystals indeed exhibit signatures of *intrinsic* high-T_c ferromagnetism, although Fe doping of just 1% is found to destroy ferroelectricity. Our effort to examine the origin of ferromagnetism using detailed first principles calculations reveals that the underlying magnetic state of this chemically pure system is intrinsically inhomogeneous and positional disorder effects must be considered as a very crucial parameter for all dilute magnetic systems, in general.

II. EXPERIMENTS

Conventional floating zone technique has been employed to grow large single crystals of four compositions (nominally 0.5, 1, 5, and 7 mole % Fe-doped $BaTiO_3$, which will be called FBT005, FBT01, FBT05, and FBT07, respectively, from now onward) under identical growth conditions. First, dense ceramic rods of nominal compositions were prepared by conventional solid state synthesis. Stoichiometric amounts of $BaCO_3$, TiO_2, and Fe_2O_3 were first weighed and then thoroughly mixed in agate mortar with ethanol and the resultant powder was then pressed under hydrostatic pressure to obtain rods of suitable dimensions, which were then calcined at 1400 °C in air for 6 h. These hard rods of high material density were used as seed and feed rods for single crystal growth in the NEC FZ SC-35H150XS floating zone furnace equipped with 1500 W power lamp. Crystal growth was carried out in flowing Ar gas with a growth rate of 7 mm/h. Seed and feed rods were counter-rotated at 42 rpm.

After the growth, the single crystals were annealed in O_2 atmosphere for a few hours in order to compensate for the possible oxygen loss due to unavoidable diffusion process that takes place during the high temperature crystal growth.

Powder x-ray diffraction measurements were carried out in a MAC Science, MXP18HF commercial x-ray diffractometer using Cu $K\alpha$ radiation. The dielectric measurements were carried out inside a commercial Quantum Design physical property measurement system using a *LCR* meter, spanning a frequency range between 50 Hz and 1 MHz, while ferroelectric loop measurements were performed using a conventional Sawyer-Tower circuit. The dc magnetization measurements were carried out in a Quantum Design superconducting quantum interference device magnetometer both as a function of temperature and as a function of magnetic field, ranging up to 5 T. X-ray absorption spectroscopy experiments were carried out at the Circular Polarization beamline (BL 4.2) of Elettra Synchrotron Center at Trieste, Italy on FBT05 and FBT07 samples.

III. CALCULATIONS

We have carried out *ab initio* calculations within the generalized gradient approximation[10] of density functional theory. A plane-wave pseudopotential method as implemented in the VASP code[11,12] was used in our calculations. Projected augmented wave potentials[13,14] were used. A 120 atom supercell of $BaTiO_3$ was considered. The unit cell dimensions were kept fixed at the experimental lattice constant of $a=5.7238$ Å and $c=13.9649$ Å,[15] while the internal coordinates were allowed to optimize so as to minimize the total energy. Single as well as pairs of Fe atoms were introduced to replace Ti2 atoms [see Fig. 4(a) for the identification of the atoms] and the formation energies in addition to the ferromagnetic stabilization energies were determined. In addition, the formation energies for intrinsic defects were also calculated. A Monkhorst-Pack grid of $2\times2\times2$ dimension was considered for the 120 atom calculations. Spheres of radius 1.0 Å were used on Fe and O for the calculation of the density of states which was done using the tetrahedron method and a denser k-point mesh of $4\times4\times4$.

IV. RESULTS AND DISCUSSION

In Fig. 1(a), we show the x-ray diffraction (XRD) patterns from all the four samples, along with the same from pure hexagonal $BaTiO_3$ and the standard pattern from the database.[16] It is to be noted that doping with only few atomic percent of transition metal in place of Ti stabilizes the hexagonal phase in $BaTiO_3$.[9] Further, the floating zone technique is known to stabilize the hexagonal phase even for the undoped $BaTiO_3$ due to the high temperature melting-quenching growth process. As a result, all the patterns appear identical, replicating the pure hexagonal $BaTiO_3$ pattern, and are found to be devoid of any impurities. The crystallinity and the crystal directions are determined using Laue diffractometry. We have also carefully determined lattice parameters of all the samples, which are shown in Figs. 1(b) and 1(c). Both the a and c parameters are found to increase with

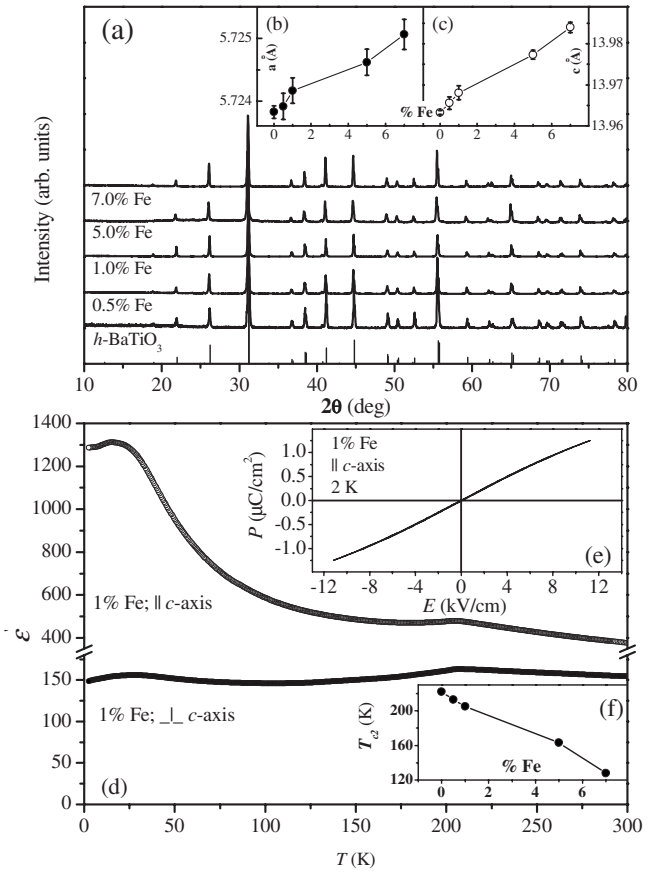

FIG. 1. (a) Powder XRD from the Fe-doped $BaTiO_3$ samples along with the same from the pure h-$BaTiO_3$ sample and the JCPDS data. Variation of lattice parameters a and c as a function of composition are shown as insets (b) and (c), respectively. In panel (d), ε' (T) data from the FBT01 sample are shown, while the 2 K P-E loop from the (001) plane has been shown in panel (e). The variation of T_{c2} with composition is exhibited in panel (f).

increasing Fe content, in accordance with the previous reports,[7,8] clearly confirming the inclusion of Fe ions inside the hexagonal $BaTiO_3$ lattice. Figure 1(d) shows the temperature dependence of permittivity (ε') from FBT01 sample collected from planes ∥ and ⊥ to (001), spanning a temperature range from 2 to 300 K, at 1 MHz frequency. The $\varepsilon_c'(T)$ behavior displays both quantitative and qualitative similarities with that of pure hexagonal $BaTiO_3$ (Ref. 17) for almost the full temperature range along with two significant dissimilarities. The well-known sharp peak in the case of hexagonal $BaTiO_3$ at around 74 K, indicating the first order ferroelectric phase transition in the same, gets completely suppressed with 1% Fe doping. The near absence of any significant P-E loop in FBT01 along the c direction at 2 K [Fig. 1(e)] at very high applied fields further confirms this. Interestingly, the higher temperature second order paraelectric to possible piezoelectric phase transition[17] ($T_{c2}=222$ K for hexagonal $BaTiO_3$) is clearly visible in the dielectric curve of FBT01, although the peak position is found to be shifted strongly down to 205 K. Identical behaviors have been observed in the other samples, where T_{c2} continues to shift almost linearly toward lower temperatures with increasing Fe doping

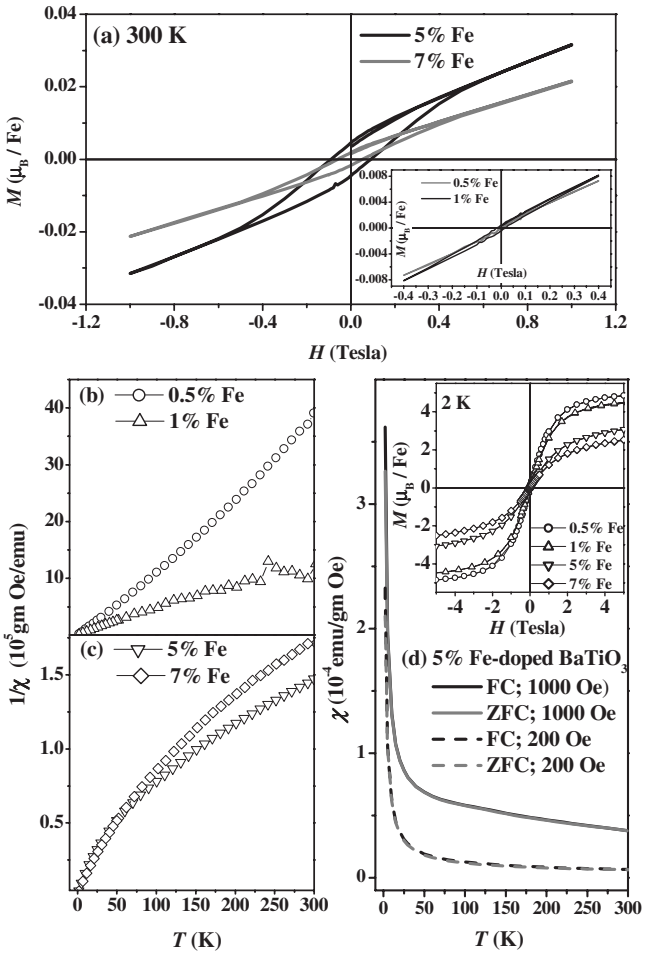

FIG. 2. (a) Room temperature $M(H)$ loops from samples FBT05 and FBT07, while the same for FBT005 and FBT01 are shown in the inset. $1/\chi$ vs T data from all the samples, collected at 1000 Oe, are shown in panels (b) and (c). In panel (d), FC and ZFC, χ vs T data from the FBT05 sample at 200 and 1000 Oe are shown, while 2 K $M(H)$ curves from all the samples are presented in the inset.

[see Fig. 1(f)]. Evidently, any description in terms of Fe clusters or Fe containing secondary phase formation will be unfit because bare physical coexistence (i.e., chemically noninteracting) of just 1% impurity phase is improbable to completely destabilize the bulk crystal distortion which leads to the first order ferroelectric phase transition. Therefore, the observed suppression of ferroelectricity in all the doped samples and the systematic variation of T_{c2} with increasing doping provide further evidence of successful incorporation of Fe ions inside the host lattice.

In Fig. 2(a), we show the results of magnetization (M) vs applied magnetic field (H) measurements from our samples at room temperature. Evidently, 5% and 7% Fe-doped samples exhibit room temperature ferromagnetism with clear $M(H)$ hysteresis loops along with possible coexisting paramagnetic and/or antiferromagnetic interactions, while FBT005 and FBT01 appear nearly paramagnetic (see inset). Thus, these results bring out a series of room temperature DMOs which appears rather clean due to its equilibrium phase diagram that, on one hand, eliminates major material related difficulties and, on the other hand, enables to grow single crystalline dilute magnets. The temperature dependence of dc magnetic susceptibility (χ) for all the samples, collected with different applied magnetic fields, qualitatively resemble the mean-field paramagnetic $\chi(T)$ pattern [see Fig. 2(d)], but most of them, especially the higher doped ones, do not follow a Curie-Weiss dependence, as can be observed from the corresponding $\chi^{-1}(T)$ dependencies in Figs. 2(b) and 2(c). It has been shown that the presence of heavy disorder is implanted in the basic idea of dilute doping, which naturally leads to a wide distribution of exchange interactions[18,19] where a significant amount of isolated, paramagnetic-type impurity spins may order only at very low T, giving rise to such unusual susceptibility curves. In the main panel of Fig. 2(d), the field cooled (FC) and zero field cooled (ZFC) $\chi(T)$ curves from the FBT05 sample, collected at 200 and 1000 Oe magnetic fields, are shown. The absence of any divergence between these two curves negates the possibility of superparamagnetic cluster formation which was often suspected to be responsible in producing spurious ferromagnetic signals in other reported DMOs.[20] The low temperature $M(H)$ curves, exhibiting near saturation for all the samples, are shown in the inset to Fig. 2(d). One important observation here is that the $M(H)$ curve at 2 K asymptotically reaches the full moment value of $5\mu_B$/Fe at 5 T magnetic field in the case of the FBT005 sample (nearly paramagnetic) and decreases rapidly with increasing Fe concentration. This reveals that the noninteracting spins, providing only a paramagnetic-type magnetization, possess Fe^{3+} high spin configuration, while the moment per "ferromagnetically interacting" Fe must be lower as the overall moment decreases with increasing ferromagnetic contribution (doping). It is also worth mentioning here that the magnetic coercivities (H_c's) are invariably found to decrease regularly and significantly with decreasing temperature in all our samples. Surely, conventional theories fail to explain this behavior, while such unusual dependence has indeed been reported in some other DMS systems,[21] although very rarely. All our attempts to analyze the $M(H)$ curves in terms of multicomponent magnetism (para+ferro) for a particular sample at different temperatures indicate that this unusual behavior is intrinsic to the ferromagnetic component and cannot be explained by just considering the presence of coexisting magnetic interactions. In the bound magnetic polaron model,[22] a systematic growth of ferromagnetic polarons at the expense of the paramagnetic spins with decreasing temperature is predicted.[23] Therefore, a gradual transition from small, single domain ferromagnetic islands at higher temperature to extended, multidomain regions at lower T might occur in this system which can affect the H_c or M_r in such unconventional way. Overall, the magnetic measurements establish the presence of room temperature ferromagnetism in Fe-doped $BaTiO_3$ single crystals with Fe concentrations being 5% or above, while the presence of spurious ferromagnetic signals from the secondary phase cluster can be, at least qualitatively, ruled out.

To check this point further, high resolution transmission electron microscopy (HRTEM) and XAS techniques were also employed, which are two very powerful tools for clari-

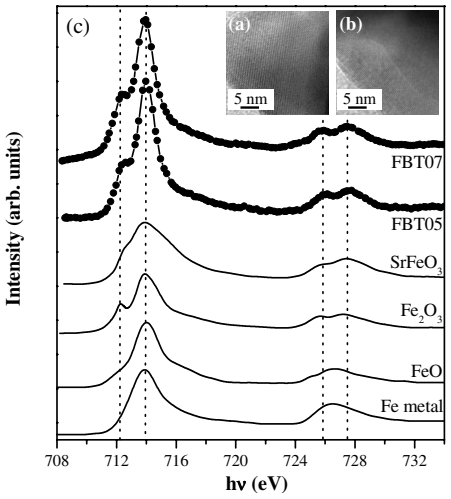

FIG. 3. High resolution TEM images from the FBT05 sample at room temperature are shown in (a) and (b). (c) Fe $2p$ XAS spectra from FBT05 and FBT07 samples along with the same reproduced from Ref. 24 for Fe metal, FeO, Fe_2O_3, and $SrFeO_3$.

fying the existence of such clusters. HRTEM measurements were performed both on powdered samples, spread over carbon grids, as well as directly on single crystal plates, thinned to electronic dimension by the use of focused ion beam. From the HRTEM studies, the presence of no impurity phase clusters could be confirmed. Two representative HRTEM images from the FBT05 sample are shown in Figs. 3(a) and 3(b), which exhibit extended, defectless lattice fringes. Fe $2p$ XAS experiments were carried out in the Circular Polarization beamline of Elettra Synchrotron Center on FBT05 and FBT07 samples. The results are shown in Fig. 3(c) along with a set of spectra from Fe with different oxidation states, acquired from different earlier reports.[24] Evidently, the experimental spectra from our samples resemble well with the same from Fe_2O_3 and do not show any similarity with the spectrum from pure Fe metal, thereby conclusively eliminating any possibility of the existence of metallic Fe clusters in these samples.

The observation of high solubility of Fe in $BaTiO_3$ is supported by our first principles calculation of formation energies of Fe in $BaTiO_3$ at various sites. While a considerable portion of the literature talks of Fe substituting the Ti2 site[8] [for the identification of different atomic sites, see Fig. 4(a)], depending on the position of the Fermi energy (E_F), we find that Fe can substitute the Ti1 site also. It is also observed that under certain chemical potential conditions, Fe substitution of interstitial[25] sites is unavoidable.

In order to investigate the relative energies of ferro- and antiferromagnetically ordered states, a second Fe was introduced in the supercell and the separations of the Fe atoms were varied to observe the tendency of Fe ions to cluster and also to test the dependence of the magnetic coupling on the interatomic distance. The essential results with two Fe atoms in the Ti2 sites in a 120 atom supercell are shown in Fig. 4(b). Interestingly, it is found that the total energy of the supercell is minimum for Fe atoms occupying the nearest-neighbor positions on the metal sublattice (NN1) and in-

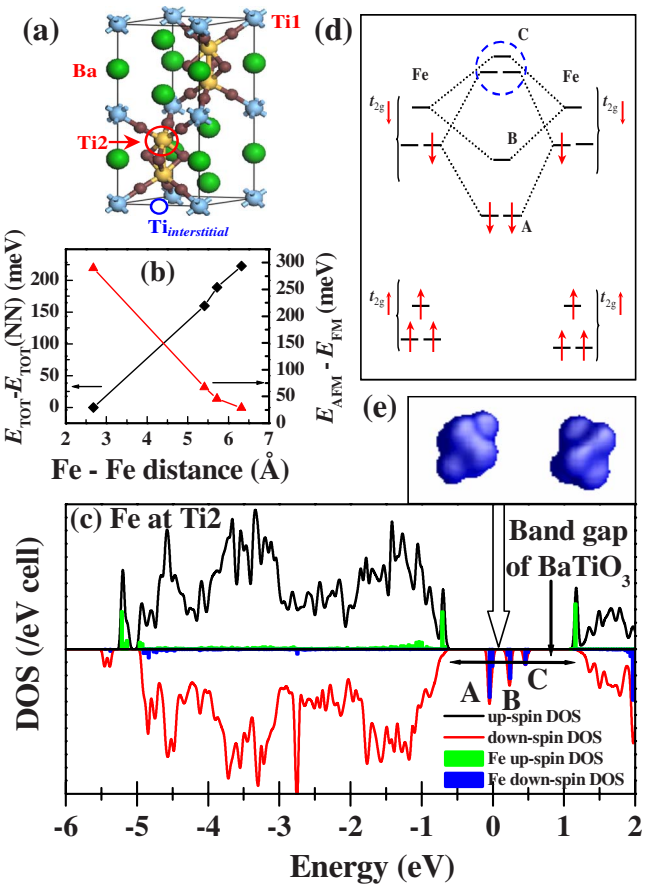

FIG. 4. (Color online) (a) The structure of hexagonal $BaTiO_3$. (b) Total energy differences for ferromagnetic Fe (Ti2) pairs relative to the nearest-neighbor (NN1) configuration (black squares, left axis) and relative ferromagnetic (FM) stability of the Fe spins [red (gray) up triangles, right axis] as a function of Fe-Fe distance. (c) Total DOS and partial DOS of Fe for a pair of ferromagnetically coupled Fe atoms at NN1 Ti2 sites in $BaTiO_3$. An energy level diagram showing the interaction between the Fe levels and the corresponding Fe molecular orbitals formed as a result of the interaction are shown in (d) and (e), respectively.

creases substantially with increasing distance (black curve), indicating a clear tendency of Fe atoms to cluster. It is to be noted that these clusters are *lattice matched* and are different from clusters formed by phase separation. Moreover, Fe at the Ti2 site evidently interacts ferromagnetically with other Fe at Ti2 sites [red (gray) curve]. This interaction is extremely strong for nearest-neighbor pairs and falls with distance, though it is still considerable (0.029 eV) for fourth neighbor Fe atoms at a separation of 6.3 Å. The mean-field T_c considering only nearest-neighbor interactions is ~600 K for a concentration of 8%. The interactions between Fe at Ti1 and Fe at Ti2 as well as between the Fe ions at Ti1 sites only are found to be very weak and, therefore, Fe ions substituting Ti1 only contribute to a paramagnetic background. Finally, the interaction between substitutional Fe at Ti2 and interstitial Fe is found to be antiferromagnetic. Hence, the low doping limit of these oxides corresponds to a soup of inhomogeneities which results in an unusual concave shape of the magnetization seen in other dilute magnetic oxides.

While investigating the mechanism of magnetism in these highly insulating systems, it is useful to understand the basic electronic structure of Fe in $BaTiO_3$. Fe favors a low spin state when it occupies the Ti2 site. As two Fe atoms (on the Ti2 site) show a strong tendency to cluster, we consider the basic electronic structure arising from two Fe atoms occupying nearest-neighbor sites. The Fe *d* projected partial density of states along with the total density of states is shown in each spin channel [Fig. 4(c)]. The schematic diagram shown in Fig. 4(d) (isovalent Ti substitution with Fe is considered, while the same mechanism will prevail for the Fe^{3+} dopants also) is useful to understand the ensuing electronic structure. The triply degenerate t_{2g} orbitals split further into doubly degenerate and singly degenerate levels due to additional crystal field effects present when the Fe atoms occupy nearest-neighbor positions. This is shown in the left- and rightmost panels of the energy level diagram presented in Fig. 4(d). The levels on the two transition metal atoms interact with each other, forming bonding and antibonding levels corresponding to features A, B, and C shown in Fig. 4(c). The real space plot of a state comprising A is shown in panel (e), which shows that the state is derived from interactions between the two Fe atoms consistent with the energy level diagram of panel (d). Evidently, in the case of a ferromagnetic arrangement of the spins at the Fe site, the interacting levels on the two sites have the same energy and only the bonding levels are filled after the interaction, resulting in an enormous energy gain. In an antiferromagnetic arrangement of the Fe spins, the energy separation between the interacting levels is determined by the exchange splitting of the interacting levels. Hence, even though the bonding levels are again occupied in the present case, the energy gain is *smaller* than that in the ferromagnetic case.

V. CONCLUSIONS

We have studied the properties of single crystalline $BaTiO_3$ doped with transition metal impurities (Fe) in the dilute limit. The system exhibits intrinsic ferromagnetism above room temperature in addition to the unusual magnetization behavior, characteristic of dilute magnetic systems, in general. Our analysis based on *ab initio* calculations suggests that disorder in doping is inherent to these systems, which eventually controls their overall magnetic nature, giving rise to many unconventional dependencies in this low doping regime. Therefore, the present system, which is largely devoid of material related uncertainties, acts as a testing ground for a sound physical understanding and establishes the standpoint that one must adopt while describing this regime.

ACKNOWLEDGMENTS

S.R. acknowledges the support from JSPS. S.R.K. acknowledges the support of the Department of Science and Technology (DST), Government of India, and the Italian Ministry of Foreign Affairs (MAE) for the Synchrotron Radiation studies. P.M. thanks DAE-BRNS, Government of India, for financial support.

*mssr@iacs.res.in
†mitsuru_itoh@msl.titech.ac.jp

[1] Y. Matsumoto, M. Murakami, T. Shono, T. Hasegawa, T. Fukumura, M. Kawasaki, P. Ahmet, T. Chikyow, S. Koshihara, and H. Koinuma, Science **291**, 854 (2001).
[2] K. Ueda, H. Tabata, and T. Kawai, Appl. Phys. Lett. **79**, 988 (2001).
[3] S. B. Ogale, R. J. Choudhary, J. P. Buban, S. E. Lofland, S. R. Shinde, S. N. Kale, V. N. Kulkarni, J. Higgins, C. Lanci, J. R. Simpson, N. D. Browning, S. Das Sarma, H. D. Drew, R. L. Greene, and T. Venkatesan, Phys. Rev. Lett. **91**, 077205 (2003).
[4] M. Venkatesan, C. B. Fitzgerald, and J. M. D. Coey, Nature (London) **430**, 630 (2004).
[5] H. Ohno, Science **281**, 951 (1998); G. A. Prinz, *ibid.* **282**, 1660 (1998); P. Ball, Nature (London) **404**, 918 (2000); S. A. Wolf, D. D. Awschalom, R. A. Buhrman, J. M. Daughton, S. von Molnár, M. L. Roukes, A. Y. Chtchelkanova, and D. M. Treger, Science **294**, 1488 (2001); A. H. Macdonald, P. Schiffer, and N. Samarth, Nat. Mater. **4**, 195 (2005).
[6] D. H. Kim, J. S. Yang, K. W. Lee, S. D. Bu, T. W. Noh, S.-J. Oh, and Y.-W. Kim, Appl. Phys. Lett. **81**, 2421 (2002); J. Y. Kim, J.-H. Park, B.-G. Park, H.-J. Noh, S.-J. Oh, J. S. Yang, D.-H. Kim, S. D. Bu, T.-W. Noh, H.-J. Lin, H.-H. Hsieh, and C. T. Chen, Phys. Rev. Lett. **90**, 017401 (2003).
[7] T. A. Vanderah, J. M. Loezos, and R. S. Roth, J. Solid State Chem. **121**, 38 (1996).
[8] I. E. Grey, C. Li, L. M. D. Cranswick, R. S. Roth, and T. A. Vanderah, J. Solid State Chem. **135**, 312 (1998).
[9] G. M. Keith, K. Sarma, N. M. Alford, and D. C. Sinclair, J. Electroceram. **13**, 305 (2004).
[10] J. P. Perdew and Y. Wang, Phys. Rev. B **45**, 13244 (1992).
[11] G. Kresse and J. Furthmüller, Phys. Rev. B **54**, 11169 (1996).
[12] G. Kresse and J. Furthmüller, Comput. Mater. Sci. **6**, 15 (1996).
[13] P. E. Blöchl, Phys. Rev. B **50**, 17953 (1994).
[14] G. Kresse and D. Joubert, Phys. Rev. B **59**, 1758 (1999).
[15] J. Akimoto, Y. Gotoh, and Y. Oosawa, Acta Crystallogr., Sect. C: Cryst. Struct. Commun. **50**, 160 (1994).
[16] JCPDS Card No. 00-034-0129 (unpublished); H. Arend and L. Kihlborg, J. Am. Ceram. Soc. **52**, 63 (1969).
[17] Y. Akishige, G. Oomi, T. Yamamoto, and E. Sawaguchi, J. Phys. Soc. Jpn. **58**, 930 (1989).
[18] M. Berciu and R. N. Bhatt, Phys. Rev. B **69**, 045202 (2004).
[19] A. Kassaian and M. Berciu, Phys. Rev. B **71**, 125203 (2005).
[20] S. R. Shinde, S. B. Ogale, J. S. Higgins, H. Zheng, A. J. Millis, V. N. Kulkarni, R. Ramesh, R. L. Greene, and T. Venkatesan, Phys. Rev. Lett. **92**, 166601 (2004).
[21] P. V. Radovanovic and D. R. Gamelin, Phys. Rev. Lett. **91**, 157202 (2003).
[22] A. Kaminski and S. Das Sarma, Phys. Rev. Lett. **88**, 247202 (2002).
[23] S. Das Sarma, E. H. Hwang, and A. Kaminski, Phys. Rev. B **67**, 155201 (2003).

[24] S. S. Lee, J. H. Kim, S. C. Wi, G. Kim, J.-S. Kang, Y. J. Shin, S. W. Han, K. H. Kim, H. J. Song, and H. J. Shin, J. Appl. Phys. **97**, 10A309 (2005); J. Okamoto, K. Mamiya, S.-I. Fujimori, T. Okane, Y. Saitoh, Y. Muramatsu, K. Yoshii, A. Fujimori, A. Tanaka, M. Abbate, T. Koide, S. Ishiwata, S. Kawasaki, and M. Takano, Phys. Rev. B **71**, 104401 (2005).

[25] If the Ti1 atoms are given by (0,0,0) and $(0,b,0)$, then the interstitial sites are at $(0,b/2,0)$.